Hindawi
Advances in Civil Engineering
Volume 2022, Article ID 7071760, 15 pages
https://doi.org/10.1155/2022/7071760

Research Article

Dynamic Performance Analysis of a Curved Cable-Stayed Bridge Based on the Direct Method and the Sensitivity-Based Iterative Method

Guanzhe Fa,[1] Leqia He,[2] Luigi Fenu,[3] and Bruno Briseghella[2]

[1]*Department of Civil Engineering, Hebi Institute of Engineering and Technology, Henan Polytechnic University, Henan, Hebi, China*
[2]*Sustainable and Innovative Bridge Engineering Research Center, College of Civil Engineering, Fuzhou University, Fujian, Fuzhou, China*
[3]*Department of Civil and Environmental Engineering and Architecture, University of Cagliari, Cagliari, Italy*

Correspondence should be addressed to Leqia He; leqia.he@fzu.edu.cn

Received 6 May 2022; Accepted 17 August 2022; Published 8 October 2022

Academic Editor: Giovanni Minafò

Copyright © 2022 Guanzhe Fa et al. This is an open access article distributed under the Creative Commons Attribution License, which permits unrestricted use, distribution, and reproduction in any medium, provided the original work is properly cited.

Curved cable-stayed bridges have been regularly accepted due to their ability to cross long spans, and a number of studies have been conducted to investigate the mechanical or dynamic performance of them. Meanwhile, currently just a few studies focus on the curved composite cable-stayed bridges. In this study, an operational modal testing and finite element model updating of a conventional straight bridge with the steel-concrete composite girder were conducted to investigate the performance of the potential methods for the model updating, which included the direct method and the sensitivity-based iterative method. Then, dynamic tests were performed for one typical curved steel-concrete composite cable-stayed bridge as the key case study. A highly refined finite element model of the bridge was developed and then calibrated based on the aforementioned methods in reference to the experimental results. Finally, the dynamic behavior of the curved steel-concrete composite cable-stayed bridge was studied based on the model. It is found that the solution accuracy of the finite element model can be improved significantly by employing the structural health monitoring technique. Moreover, by using the iterative method, the solutions of the updating parameters are generally more accurate compared with the solutions of the direct method. Nevertheless, when the appropriate choices are made for the algorithmic parameters, both methods can lead to the updated models with satisfactory numerical analysis results as compared to the experimental data.

1. Introduction

During the last decades, curved cable-stayed bridges have been regularly accepted due to their ability to cross long spans. Cable-stayed bridges are being built in more particular styles for both structural reasons and aesthetic considerations [1]. In addition to the many regular symmetric cable-stayed bridges with spans exceeding 1000 m, the asymmetric bridge or other designs (e.g., curved cable-stayed bridges) become more and more common. Therefore, the curved cable-stayed bridges due to their interesting dynamic characteristics require further investigation.

The primary purpose of the designers to choose curved bridges is to unite the curved structures with their surrounding environment and to create the architectural style for future development of the cites. It is hoped that the designers of the future cites can provide a direction or guidance in the design process, assuring that the aesthetic properties of the bridges are more effective [2]. However, such kind of bridges typically with several special geometric shapes might provide a different mechanical or dynamic performance as compared to the conventional straight bridges [3].

Currently, a series of studies have focused on the performance of the cable-stayed bridges. Heyrani Moghaddam

et al. [4] proposed a seismic evaluation procedure for a cable-stayed bridge based on the energy balance concept, which could estimate its seismic responses with good accuracy. Choi et al. [5] investigated the ultimate behavior of steel cable-stayed bridges and found that the inelastic buckling analysis was an effective approximation method for obtaining the ultimate load capacity of the long span cable-stayed bridges. Hassan et al. [6] developed a robust design optimization technique to achieve the minimum cross-sectional areas of stay cables, and the proposed optimization technique was assessed by applying it to the cable-stayed bridge of a practical size. Wei et al. [7] developed an efficient seismic fragility analysis framework based on the endurance time method (ETM) for cable-stayed bridges under scour and earthquake, and the ETM was found to be able to significantly reduce computational efforts without compromising the accuracy of analysis results. Kim et al. [8–10] investigated the structural and ultimate behaviors of steel cable-stayed bridges with parametric analysis. It was found that rational ultimate analysis method was able to provide an accurate prediction on the ultimate behavior of steel cable-stayed bridges.

Although a number of studies were conducted to investigate the mechanical or dynamic performance of the cable-stayed bridges, among them just a few focused on the curved composite cable-stayed bridges. For instance, Bhagwat et al. [11] evaluated the dynamic behavior of both straight and curved cable-stayed bridges and found that the induced curvature in decks could introduce coupling of different modes of the curved bridges, whereas the modes of the straight bridges were quite distinct. Ferreira and Simões [12] conducted an optimum design of curved cable-stayed footbridges with control devices using the three-dimensional model and found that the optimum tower's height-to-span ratio of the curved bridges remained constant at around 0.18 for all designs.

Considering the limited experimental and analytical studies on the curved composite cable-stayed bridges, in order to better understand the dynamic performance of such a kind of bridges, it is necessary to investigate their dynamic behavior by considering both serviceability and ultimate working conditions. In this study, an operational modal testing and finite element (FE) model updating of a conventional straight bridge with the steel-concrete composite girder were conducted to verify the potential methods for the model updating, which included a direct method (i.e., the Douglas-Reid algorithm) [13] and a sensitivity-based iterative method (i.e., the Trust-Region-Reflective algorithm) [14]. For the direct method, the approximation of the numerical modal properties is made with a second-order polynomial around the so-called reference point (consisted of the updating parameters) between the predefined upper and lower limits of the uncertain parameters. Once the objective function is obtained with the aforementioned approximation, modal analysis of the FE model can be avoided, which is usually the most computationally expensive parts in the model updating process. On the other hand, for the iterative method, the numerical properties of the FE model have to be repeatedly computed during the updating process at each iteration with the updated values of the design variables (the updating parameters). Strictly speaking, both algorithms are iterative methods to solve complex nonlinear numerical problems. The concepts of the direct and iterative methods are derived by following the general framework of the FE model updating process as defined by Friswell and Mottershead [15]. It implies that a direct method does not require the numerical solution of the FE model once the objection function of the optimization problem is defined, whereas an iterative method repeatedly solves the FE model while seeking for the optimum solution in the FE updating process. Herein, both methods are intended to solve the following nonlinear least-squares problem as encountered in the FE model updating process:

$$\mathbf{P}^* = \underset{\mathbf{P}}{\operatorname{argmin}} \sum_i w_{m,i}\left(\varepsilon_{m,i}(\mathbf{P})\right)^2, \tag{1}$$

where $\varepsilon_{m,i}$ denotes the residuals between the experimental and numerical modal data m. Without loss of generality, it is considered that $\varepsilon_{\lambda,i}(\mathbf{P}) = (\lambda_i(\mathbf{P}) - \tilde{\lambda}_i)/\tilde{\lambda}_i$, with $\lambda_i = \omega_i^2 = (2\pi f_i)^2$ and $\varepsilon_{z,i}(\mathbf{P}) = 1 - MAC_i$ for $i \in \{1, 2, \ldots, n\}$ with n being the number of modes. The upper tilde denotes the experimental values. And the MAC values are calculated between the numerical mode shapes and their experimental counterparts according to [16]. In addition, $w_{\mathrm{m},i}$ represents the weighting factors. Then, taking a curved cable-stay bridge, known as the Marghera Bridge in Venice, Italy, as the key case study, the results of the dynamic tests were presented. A highly refined FE model of the bridge was developed and then calibrated in reference to the experimental results based on both the aforementioned methods. Finally, the dynamic behavior of this curved steel-concrete composite cable-stayed bridge was studied based on the calibrated model.

Figure 1: The Magaz bridge.

2. Verification of the Methods for the Model Updating

In this section, a conventional steel-concrete composite bridge is updated with respect to the experimental data in order to investigate the performance of both the direct and iterative methods. The study of the chosen straight bridge allows for a better understanding of the applicability and limitations of the selected methods before they are applied to the more complicate curved bridge.

2.1. Bridge Introduction. The studied bridge is located in Magaz, Spain, with 10 km from Palencia over "Autovia de Castilla" that goes from Palencia to Burgos.See Figure 1. The

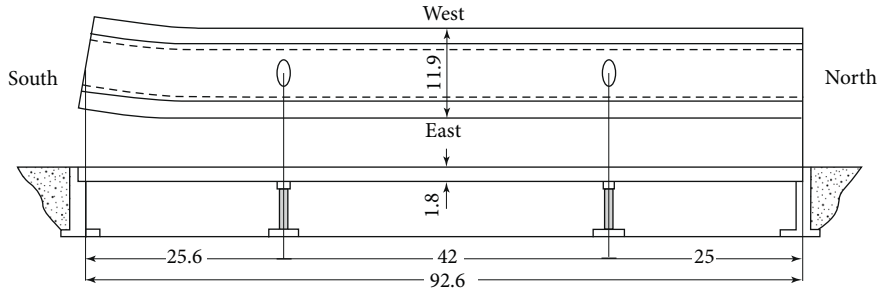

Figure 2: Technical drawing with the main geometrical features of the Magaz bridge (units in meter).

(a) (b)

Figure 3: Details of the construction: the abutment (a) and the pier (b) of the Magaz bridge.

deck was designed as a classical composite structure of steel and reinforced concrete, with a lower steel box girder of trapezoidal shape including internal reinforcing structures and stiffening braces. And the upper slab of reinforced concrete was connected by shear studs to the steel girder. The total length of the bridge is 92.6 m, with the main span of 42 m and two side spans of 25.6 m and 25 m, respectively (see Figure 2). The width of the slab is 11.9 m and the thickness is 150 mm in its cantilever part and 300 mm in its central part. The bridge is not completely straight, but it has the slight curvature on the south lateral span, which leads to the coupling of the bending and torsional modes of the structure. The steel box and the concrete deck are completely disconnected from the accessing ramps, and the steel railing has connection points only on the lateral part of the concrete sidewalks. More details of the construction are given in Figure 3.

Although the developed FE model has several nonlinear components, the linear portion of the stiffness matrix has been used for the modal analyses that were carried out in this study. In addition, all selected physical parameters were linear in nature for the purpose of model calibration. A summary of the numerical modal results that were obtained with the initial FE model before calibration is presented in Table 1. The vibration of the three-span bridge is characterized with vertical bending and torsion modes. The calculated undamped natural frequencies are usually widely spread except some of the higher modes. See, for instance, in Table 1, Mode 7 and Mode 8. The numerical modal information that was given by the initial FE model provided a guidance for the design of the testing plan as given in the next subsection.

2.2. Finite Element Simulation. A detailed 3D FE model was developed to provide a realistic simulation of the bridge. An isometric view of the FE model of the bridge is shown in Figure 4. It was developed by using the following assumptions: (1) The concrete slabs were simulated using eight-node solid elements. The elastic modulus of the concrete slabs was 28.0 GPa. (2) The steel girders were simulated using four-node shell elements and the properties of the steel grade were the plates S355 for the girders and S275 for the other structural components of the bridge. (3) Steel stringers, transverse cross-beams, and bracing elements of the deck were modelled by two-node 3D beam elements and the modulus of elasticity and the weight per unit volume of the steel were assumed as 205 GPa and 78.5 kN/m^3, respectively. (4) Rigid links (without mass density) were used between the concrete slab and the steel girder. (5) The piers are simulated with 3D beam elements and the abutments are replaced with rigid constraints (the deck is movable in the longitudinal direction at one side of the bridge and fixed at the other side).

2.3. Ambient Vibration Testing. During the ambient vibration tests, a grid of ninety measurement points were employed with the vertical accelerations being recorded. As mentioned before, the testing plan was developed according to the results obtained from the finite element modal

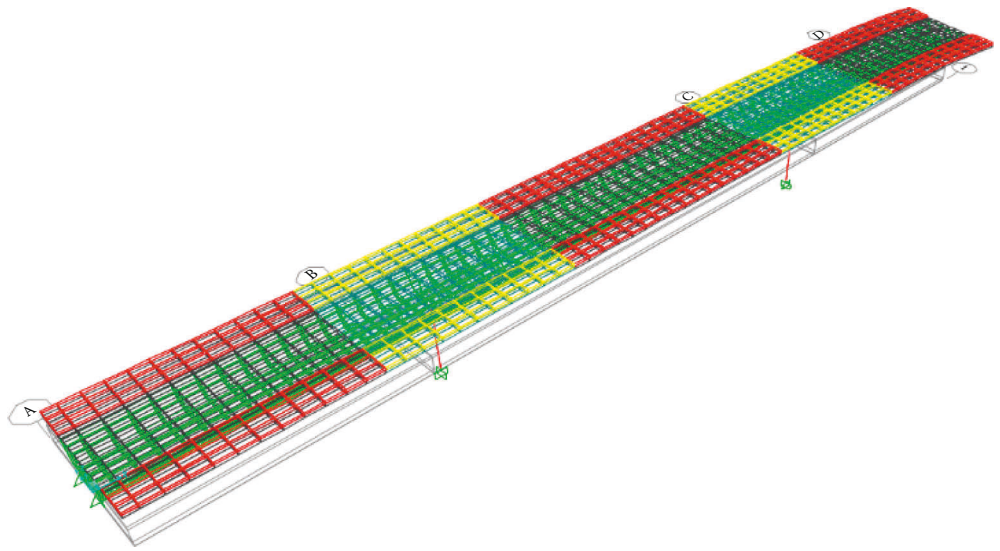

Figure 4: Finite element model of the Magaz bridge.

Table 1: Comparison between the experimental and the numerical modes for the initial model.

Experimental results		Initial FEM results				Type
Mode	f_{exp} (Hz)	Mode	$F_{FE\text{-}ini}$ (Hz)	Δf (%)	MAC	
1	2.489	1	2.463	−1.02	0.896	Vertical bending
2	4.833	2	4.569	−5.47	0.718	Vertical bending
3	5.417	3	6.100	12.60	0.904	Vertical bending
4	7.089	4	6.951	−1.94	0.824	Vertical bending
5	8.290	5	7.223	−12.86	0.687	Torsion
6	10.130	6	9.484	−6.37	0.885	Torsion
7	11.312	7	11.335	0.20	0.774	Vertical bending
8	12.137	8	11.730	−3.35	0.202	Torsion
9	15.319	9	15.560	1.57	0.440	Torsion

Note. $\Delta f = (f_{FE-ini} - f_{exp})/f_{exp}$.

analysis. The testing procedure was divided into nine setups, due to the limited channel number of the acquisition system compared to that of the measurement points. Operational modal analysis was performed on the data of around fifteen minutes for each setup, which was acquired by a self-developed wireless system of the UPM [17]. These data were sampled at a frequency of 3906.25 Hz, which is a very high frequency for vibration measurements of the civil structures. Data preprocessing and system identification were performed by using MACEC, the MATLAB toolbox for structural system identification, developed by the Structural Mechanics Section of the KUL [18].

System identification was based on the covariance-driven Stochastic Subspace Identification algorithm (SSI-cov) [19, 20]. From the observation of all the nine stabilization diagrams obtained from the different setups, totally nine experimental modes and the corresponding modal parameters were identified. These identified modes were present in all the experimental setups, which shows a good stability with respect to the system order variation. The first six identified mode shapes are illustrated in Figure 5. In addition, the comparison between the experimental and the initial FE modes is given in Table 1. It is noted that the linear similarity of the mode shapes, as indicated by the MAC values, shows a good result for the first seven identified modes and similarly do the relative differences in frequency except for Mode 3 and Mode 5.

2.4. Finite Element Model Updating. Both the Douglas-Reid algorithm method (i.e., the direct method) and the sensitivity-based iterative algorithm method were used for the FE model updating procedure. For more details of the methods and their implementation, we refer the reader to [21]. As the first step in the calibration process of the FE model, a parametric study was performed to identify the most sensitive parameters affecting the FE model-computed modal parameters (i.e., the natural frequencies) [22]. After a careful consideration of the initial FE model together with the engineering judgements, ten parameters were selected in the bridge FE model for the sensitivity analysis. These parameters were related to either the supporting conditions of the bridge or the mass/stiffness properties, as listed in Table 2. There were no data found in the engineering drawings about the thickness of the asphalt overlay on the bridge. Their effects were included in the model as the equivalent mass

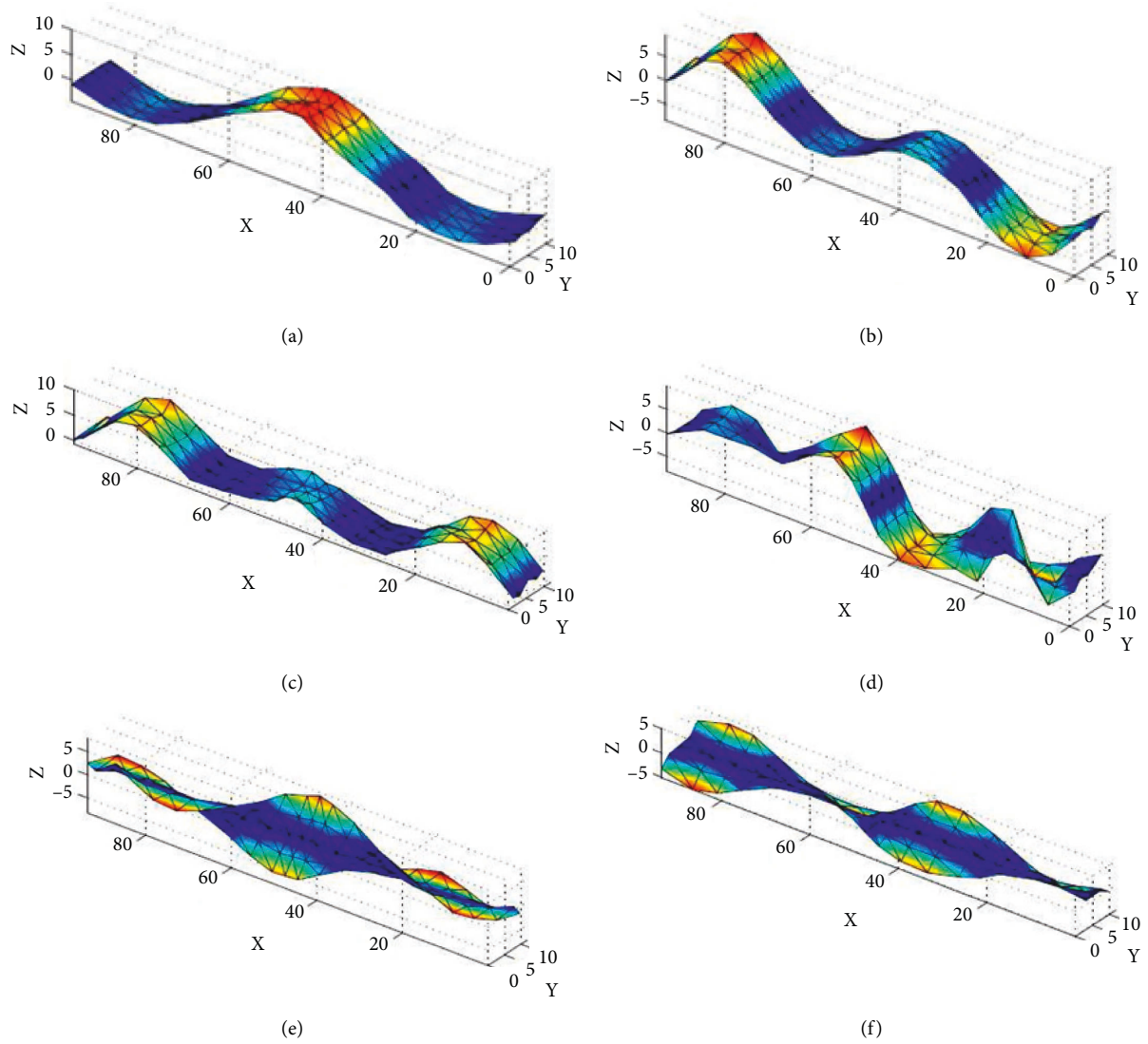

Figure 5: Representative vibration modes of the experimental results. (a) Mode 1: $f_{exp} = 2.489$ Hz, (b) Mode 2: $f_{exp} = 4.833$ Hz, (c) Mode 3: $f_{exp} = 5.417$ Hz, (d) Mode 4: $f_{exp} = 7.089$ Hz, (e) Mode 5: $f_{exp} = 8.290$ Hz, and (f) Mode 6: $f_{exp} = 10.130$ Hz.

Table 2: List of the parameters considered for the FE model updating process.

No.	Parameters	Mean	Min	Max
1	EM of the sidewalks at the middle span (kg/m^2)	360	288	432
2	EEM of the sidewalks at the middle span (GPa)	32.4	25.9	38.9
3	EM of the sidewalks at the side spans (kg/m^2)	360	288	432
4	EEM of the sidewalks at the side spans (GPa)	32.4	25.9	38.9
5	EM of the slabs at the middle span (kg/m^2)	720	576	864
6	EEM of the slabs at the middle span (GPa)	36	28.8	43.2
7	EM of the slabs at the side spans (kg/m^2)	720	576	864
8	EEM of the slabs at the side spans (GPa)	36	28.8	43.2
9	Vertical stiffness of pier 1, north (kN/m)	7,883,000	3,941,500	11,824,500
10	Vertical stiffness of pier 2, south (kN/m)	7,883,000	3,941,500	11,824,500

Notes: EM stands for the equivalent mass; EEM stands for the equivalent elastic modulus.

and stiffness with a weighting factor that changes the mechanical properties of the concrete slabs. Similar consideration was made concerning the weight and elastic modulus of the sidewalks, such as a weighted value of the parameters taking into account the pavements as well as the railing. A lower and upper range of ±20% was chosen as the variation

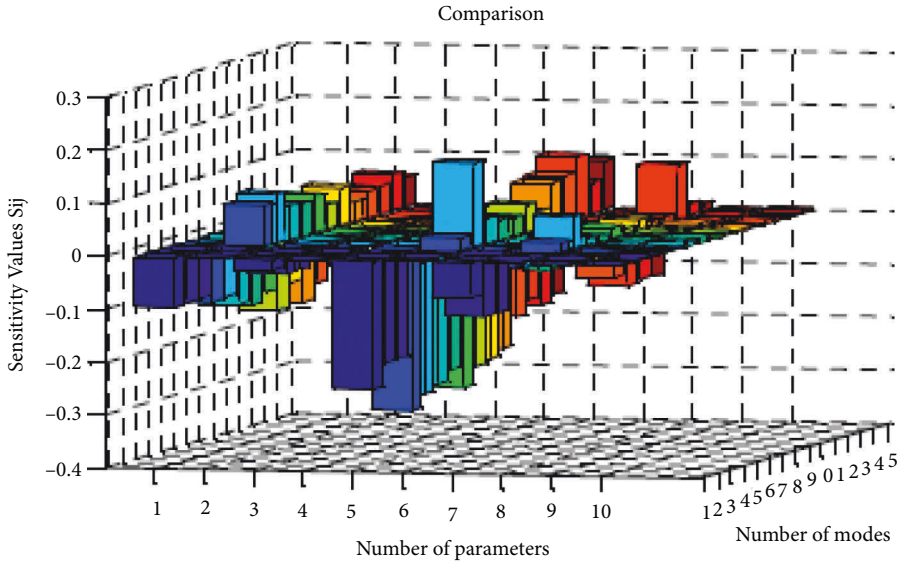

Figure 6: Results of the sensitive analysis of the selected parameters.

Table 3: Numerical modal results in comparison to the experimental counterparts.

No.	f_{exp} (Hz)	$f_{FE\text{-}ini}$ (Hz)	$\Delta f_{FE\text{-}ini}$ (%)	MAC	$f_{FE\text{-}D}$ (Hz)	$\Delta f_{FE\text{-}D}$ (%)	MAC_D	$f_{FE\text{-}I}$ (Hz)	$\Delta f_{FE\text{-}I}$ (%)	MAC_I
1	2.489	2.463	−1.02	0.90	2.476	−0.51	0.91	2.492	0.13	0.92
2	4.833	4.569	−5.47	0.72	5.035	4.18	0.84	4.813	-0.41	0.88
3	5.417	6.100	12.60	0.90	5.743	6.02	0.91	5.633	3.99	0.94
4	7.089	6.951	−1.94	0.82	6.963	−1.77	0.86	6.949	-1.97	0.91
5	8.290	7.223	−12.86	0.69	7.834	−5.49	0.79	7.991	-3.60	0.84
6	10.130	9.484	−6.37	0.89	9.583	−5.40	0.88	9.774	-3.51	0.93
7	11.312	11.335	0.20	0.77	11.42	0.95	0.83	11.372	0.53	0.87

Note: $\Delta f_{FE-ini} = (f_{FE-ini} - f_{exp})/f_{exp}$; $\Delta f_{FE-D} = (f_{FE-D} - f_{exp})/f_{exp}$; $\Delta f_{FE-I} = (f_{FE-I} - f_{exp})/f_{exp}$.

for the sensitivity analysis. Modal analyses were then performed using the lower and upper bound values of the selected parameters as listed in Table 2.

The results of the sensitive analysis are presented in Figure 6 for the selected 10 parameters. The parameters that represent the stiffness of the piers show a lower sensitivity compared to the parameters associated with the mass and stiffness properties of the bridge. Finally, five of them that illustrate a satisfactory sensitivity are selected as the design variables of the optimization process. They include the equivalent mass (EM) of the slabs at the middle span, EM of the slabs at the side spans, equivalent elastic modulus (EEM) of the sidewalks at the middle span, EEM of the sidewalks at the side spans, and the vertical stiffness of the piers. In particular, the stiffness of pier 1 and that of pier 2 are grouped into one parameter in the updating process due to the identical construction and their similar values of sensitivity.

The experimental modal data were introduced as the target of the FE updating for both the aforementioned methods, which included the first seven modes as listed in Table 1. In a greater detail, the goodness of the model updating results also depends on the values of the weighting factors, w_λ and w_z, which are used to balance the importance of the modal frequency and mode shape parts of the objective function, respectively (see (1)). The value of w_λ was adopted as 1.0, and the value of w_z was adopted as 2.0. A discussion about the influence of the weighting factors goes beyond the scope of this study. An interested reader might find some general information in [22] and the findings about a specific case study in [23]. The reference or the initial values of the updating parameters for the direct method and the iterative method, respectively, were the mean values as listed in Table 2. The final FE-updated modal frequencies are presented in Table 3. The differences between the identified and initially calculated modal frequencies vary in magnitude from 0.2% for the seventh mode to 12.86% for the fifth mode. Totally seven modes between 2.40 Hz and 11.50 Hz were found with a good correspondence to the experimental results after the FE model updating. A summary of the numerical modal results of the updated FE models is listed in Table 3 in comparison with their experimental counterparts. The numerical modal results of the reference/initial FE model (with the mean values of the selected parameters in Table 2) were also included. The subscripts *ini*, *D*, and *I* denote the initial model, the updated model with the direct method, and the updated model with the iterative method, respectively. f_{exp} dneotes the experimental natural frequencies.

As listed in Table 3, the solutions of the updated model of the iterative method are generally more accurate than those

Figure 7: The curved cable-stayed bridge of the Porto Marghera (Venice, Italy).

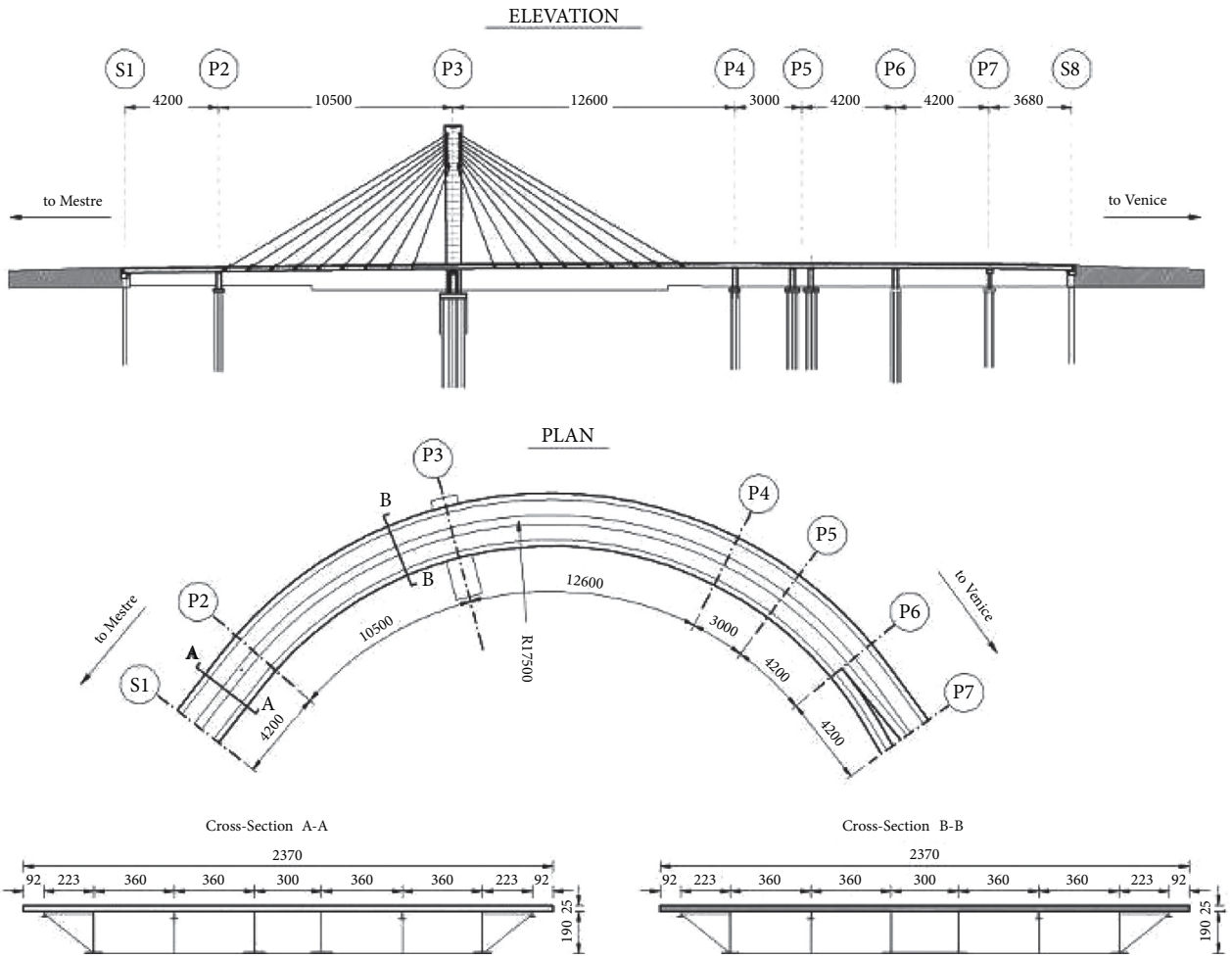

Figure 8: Plan view, elevation view, and typical deck cross sections (units in cm).

of the updated model obtained by the direct method as compared to the experimental results. As an indicator of the model quality, the average difference in frequency is defined as $\Delta\overline{f} = \sqrt{(\sum \Delta f_i^2)/n}$ and the average MAC value is defined as $\overline{MAC} = \sum MAC_i/n$ with n being the number of modes. It is found that, for the initial model, $\Delta\overline{f}_{ini} = 7.83\%$ and $\overline{MAC}_{ini} = 0.81$. The values are improved to $\Delta\overline{f}_D = 4.41\%$ and $\overline{MAC}_D = 0.86$ for the updated model with the direct method and $\Delta\overline{f}_I = 2.65\%$ and $\overline{MAC}_I = 0.90$ with the iterative method. Nevertheless, in the case where a good choice of the reference/initial values is made, both methods can lead to the models with the satisfactory modal results as compared to the experimental data. In addition, the relatively lower computational costs of the direct method shall also be noted, which are around one-tenth of those of the iterative method for the current case study.

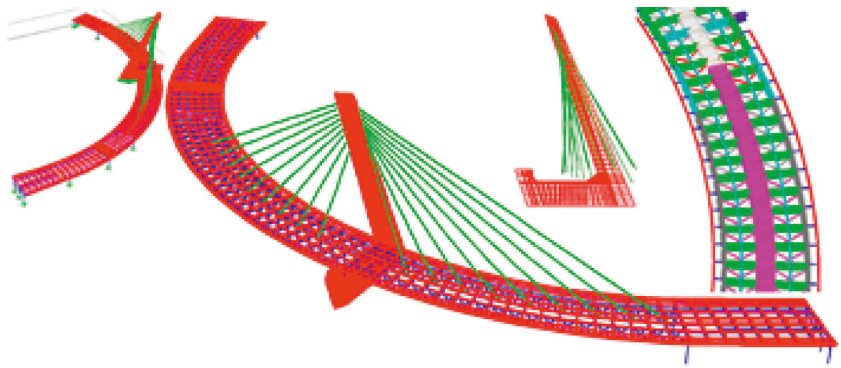

Figure 9: Finite element model of the curved composite stay-cabled bridge, the Marghera bridge.

3. Key Studied Curved Steel-Concrete Composite Cable-Stayed Bridge

3.1. Marghera Cable-Stayed Bridge. The Porto Marghera bridge is characterized by an inclined L-shape prestressed concrete pylon, a single set of cables with spatial arrangement, and a curved steel-concrete composite deck, as shown in Figure 7. The bridge was constructed to cross the West Industrial Canal in the Marghera basin and to complete the road link between the national highway and the port areas. The bridge has a total length of 387 m of six spans ($42\,m + 105\,m + 126\,m + 30\,m + 42\,m + 42$ m), with the first span on a straight alignment and the others curved with a radius of 175 m. Plan view, elevation view, and typical cross sections of the deck are shown in Figure 8. The two main spans of the bridge are arranged on a cable-stayed layout with the stays arranged on a single plane, which is connected to the center of the cross section of the box girder. The total width of the deck is 23.70 m for two traffic lanes and three pedestrian walkways.

The structural arrangement of the deck consists of a composite steel and concrete continuous girder, covering all the six spans. In such a frame, two main cross sections can be identified: the first one, adopted at the end-spans, consists of four double-T steel girders, while the second one, characterizing the central spans, consists of two outer double-T steel girders and one central girder of box section. The girders are stiffened by transverse cross-beams.The steel girders and cross-beams have a height of 1.90 m and are connected to an overlaying cast-in-place concrete slab, with a thickness of 25–27 cm (Figure 8). The cast-in-place prestressed concrete inclined tower played a determining role in the conceptual and executive design of the bridge. The tower with a height of roughly 75 m is characterized by a triangular cross section varying its dimensions along the inclined longitudinal axis. In a specific case, the base of the cross section enlarges upward so as to provide a more suitable anchorage zone for the stays. A more detailed introduction of the Porto Marghera bridge is provided by Briseghella et al. [25].

3.2. Finite Element Simulation. The geometry of the bridge was defined in CAD software accounting for the curved layout of the deck and its transverse slope, which was different in each bridge segment from S1 to P7. Furthermore, in the definition of the steel members of the deck, the different types of beam cross section were associated with different CAD layers. All the beam elements were represented along the centroid axis, and the vertical rigid offsets were drawn to connect the nodes of beam elements to the nodes of shell elements in order to model the steel-concrete composite action. The mesh was already virtually defined manually. Finally, the tower and its basement were drawn in order to allow the later modelling by solid elements.

The CAD model was subsequently transferred to the software SAP2000 with the geometrical information to create the numerical model of the bridge. The FE model was formulated by using the following assumptions: (1) Three-node and four-node shell elements were used to model the concrete slab. (2) Tower P3 and its basement were modelled by solid elements. (3) The concrete piers P2 and P4–P7 were modelled by two-node 3D beam elements. (4) The weight per unit volume and Poisson's ratio of the concrete were held constant and equal to 25.0 kN/m^3 and 0.2, respectively. (5) An additional weight per unit surface of 1 kN/m^2 was considered for the deck slab to account for the effects of the asphalt pavement and walkways. (6) Steel stringers, transverse cross-beams, and bracing elements of the deck were modelled by two-node 3D beam elements. (7) Rigid links (without mass density) were used for connectivity between the concrete slab and the steel girders. (8) The stays were modelled by 3D truss elements. (9) The boundary conditions between piers P2–P7 and the foundation were assumed to be fixed. The finite element model of the Porto Marghera bridge, or simply the Marghera bridge, is shown in Figure 9.

The FE model accounted for the geometric and structural complexity of the viaduct as much detailed as possible. The main uncertainties are related to the actual behavior of the constraints and to Young's modulus of the concrete elements, which are, namely, the deck (ED), piers P2–P4-P5-P6-P7 (EP), and the tower and its basement P3 (ET). Hence, some preliminary dynamic analyses were performed to investigate the theoretical modal parameters, which might be identified with an ambient vibration testing campaign. A summary of the numerical modal characteristics of the original model, denoted by O, is presented in Table 4. In the

Table 4: Comparison of the numerical and experimental frequencies for different modelling choices.

	f_{2011}	O	Δf (%)	$+CF$	Δf (%)	E	Δf (%)	$+CE$	Δf (%)	$+CEA$	Δf (%)
B1	0.64	0.67	6.2	0.68	6.8	0.71	11.1	0.71	11.7	0.68	7.4
B2	1.00	0.96	−3.1	0.97	−2.4	0.97	−2.4	0.98	−1.7	0.97	−2.2
B3	1.14	1.20	4.9	1.20	5.0	1.25	9.4	1.25	9.5	1.19	4.7
T1	1.39	1.30	−6.2	1.30	−6.2	1.37	−1.3	1.37	−1.2	1.31	−5.8
M1	1.52	1.59	4.7	1.59	4.7	1.74	14.1	1.74	14.4	1.67	9.1
T2	1.60	1.65	2.8	1.65	2.8	1.79	11.7	1.79	11.7	1.74	6.1
B4	1.96	2.17	10.6	2.17	10.7	2.29	16.5	2.29	16.5	2.20	12.0
T3	2.65	2.68	1.4	2.68	1.4	2.99	13.0	2.99	13.0	2.90	7.2
T4	n.a.	3.16	—	3.16	—	3.52	—	3.52	—	3.41	—
T5	4.07	3.78	−7.2	3.78	−7.2	4.13	1.4	4.13	1.4	3.96	−3.4
T6	4.95	4.58	−7.6	4.58	−7.6	5.00	1.0	5.00	1.0	4.80	−3.9
T7	5.33	5.34	0.2	5.34	0.2	5.76	8.1	5.76	8.1	5.54	3.0
T8	5.63	5.70	1.4	5.70	1.4	5.89	4.7	5.89	4.7	5.63	−0.5
T9	5.88	6.11	3.9	6.11	3.9	6.68	13.6	6.68	13.6	6.40	8.1
T10	6.84	6.73	−1.5	6.73	−1.5	7.10	3.9	7.10	3.9	6.81	−1.0

Note: O represents the original model; $+CF$ represents the model considering the cable forces; E represents the model with the slab modelled with solid elements instead of shell elements; $+CE$ represents the model considering the cable forces and with the slab modelled with the solid elements; $+CEA$ is developed from $+CE$ by taking into account the effects of the asphalt layer.

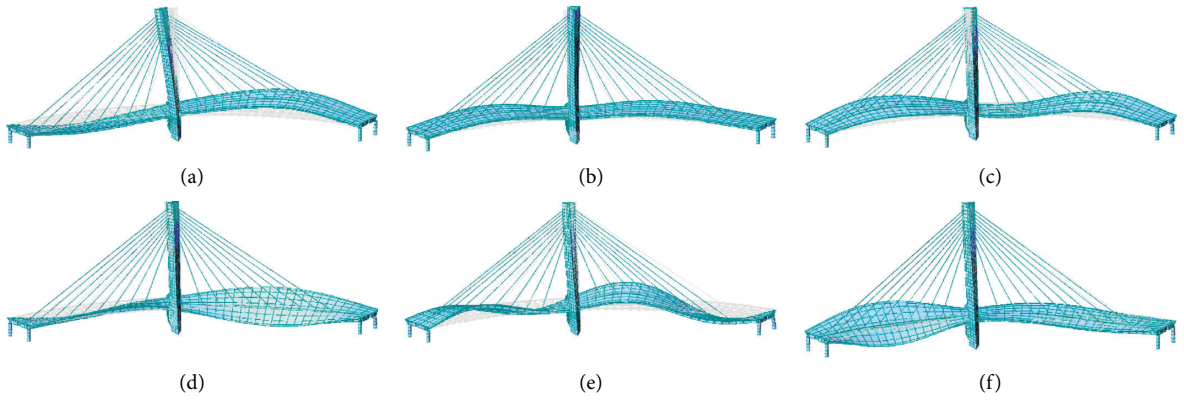

Figure 10: Selected vibration modes of the FE model of the Marghera bridge. (a) $f_{FEM} = 0.67$ Hz (B1). (b) $f_{FEM} = 0.96$ Hz (B2). (c) $f_{FEM} = 1.20$ Hz (B3). (d) $f_{FEM} = 1.30$ Hz (T1). (e) $f_{FEM} = 1.59$ Hz (M1). (f) $f_{FEM} = 1.65$ Hz (T2).

table, B represents the bending-dominated modes, T represents the torsion-dominated modes, and M represents the mixed modes of bending and torsion. In these analyses, the ED, ET, and EP ranging from 34 to 42 GPa were firstly assumed. Then a first manual tuning conducted by Gentile [26] provided the values of ED, ET, and EP as 40.0 GPa, 40.0 GPa, and 36.0 GPa, respectively. Selected mode shapes of the original model are shown in Figure 10.

In Table 4, the modal characteristics of the FE model are also compared with the experimental data, which will be described with more details in the next subsection. It can be observed that all the experimental modes are reproduced by the model with fairly good accuracy. The relative error of natural frequencies is defined as the difference between the calculated and the experimental values divided by the experimental one. The errors are rather small in magnitude, which are generally less than 5%, expect for modes T1, B4, T5, and T6. The original model (O) was then slightly modified to investigate the influence of different modelling assumptions and simplifications on the numerical modal results. It includes the effects of the cable forces ($+CF$), modelling choices of the concrete slabs (E), a combination of the aforementioned two effects ($+CE$), and last but not least the asphalt layer ($+CEA$). In particular, the cable forces considered in the FE model were identified by testing. In each case, the correlation between the numerical and experimental modal data seems to provide a sufficient verification of the main assumptions adopted in the model. It should be noted that the effects of the cable forces on the dynamic behavior, as predicted by the FE model, are smaller than those by utilizing the different element types of the slab and adding the asphalts layer as the additional mass. The above results highlight that the model represents a fairly good approximation of the real structure and could surely be adopted either as the baseline model for long-term monitoring or as the starting point for calibration of the more accurate FE model with high fidelity.

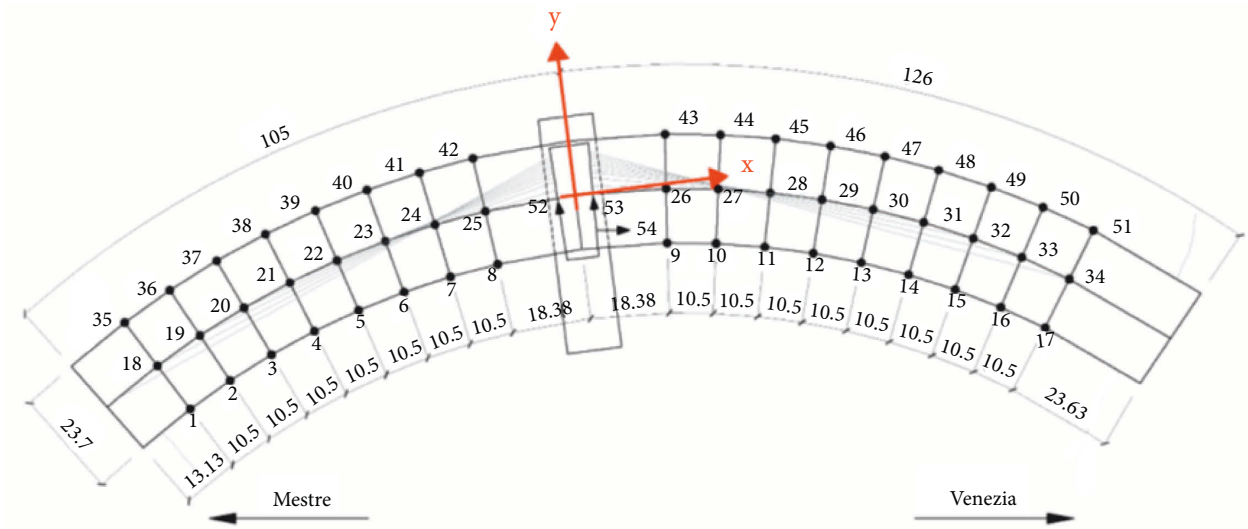

Figure 11: The measurement nodes on top of the bridge deck and on the tower (units in meter).

Table 5: Comparison of the experimental modal data between 2010 and 2011.

Mode	f_{2010} (Hz)	f_{2011} (Hz)	$\triangle f$ (%)	MAC	Type
1	0.635	0.635	0.0	0.99	Vertical bending
2	0.996	0.996	0.0	0.98	Vertical bending
3	1.143	1.143	0.0	0.96	Vertical bending
4	1.387	1.387	0.0	1.00	Torsion
5	1.523	1.523	0.0	0.98	Bending-torsion
6	1.602	1.602	0.0	0.99	Bending-torsion
7	1.953	1.963	0.5	0.99	Vertical bending
8	2.637	2.646	0.3	0.98	Torsion
9	3.174	n.a.	—	—	Torsion
10	4.053	4.072	0.5	0.95	Torsion
11	4.932	4.951	0.4	0.84	Torsion
12	n.a.	5.332	—	—	Torsion
13	5.596	5.625	0.5	0.84	Torsion
14	n.a.	5.880	—	—	Bending-torsion
15	6.826	6.840	0.2	0.97	Torsion

3.3. Ambient Vibration Testing. The operational modal analysis of the Marghera bridge included extensive measurements of the ambient vibration responses induced by the environmental actions. Ambient vibration tests were conducted in both 2010 and 2011 by using the 16-channel data acquisition system with 14 uniaxial piezoelectric accelerometers. Each sensor was connected with a 1 m long short cable to the power amplifier, which provided the power for the accelerometer's internal amplifier, signal amplification, and selective filtering. Two-conductor cables connected the power supplies to the data acquisition board. In order to obtain a satisfactory spatial description of the bridge's mode shapes, the accelerations were measured in 51 selected points of the deck, while only one cross section of the tower (uprising the deck of about 15 m) was instrumented by three sensors (nos. 52–54). Figure 11 shows a schematic diagram of the sensor layout. The tests were performed in a total of three setups. Moreover, the cable forces of the Marghera bridge were identified using a novel sensing technique with high accuracy during the dynamic testing [27]. For this reason, the cables forces were supposed to be known and not considered as the uncertain parameters in the numerical investigation. See more details about the identified natural frequencies of the cables in [28].

The identification of modal parameters from the ambient vibration data was carried out by using the output-only method, namely, the Frequency Domain Decomposition (FDD) algorithm [28]. The two sets of mode data obtained in 2010 and 2011 were compared in terms of the relative differences in natural frequency and the mode shapes as measured by the MAC values (see Table 5). The analysis of the acceleration signals recorded on the bridge deck and on the tower led to the identification of thirteen modes in 2010 and fourteen modes in 2011. Their relative differences in natural frequency are almost negligible for the first six modes, and the maximum value of the difference is less than 1% even for the higher modes. Due to the excitation levels, some modes might not be well excited and therefore not

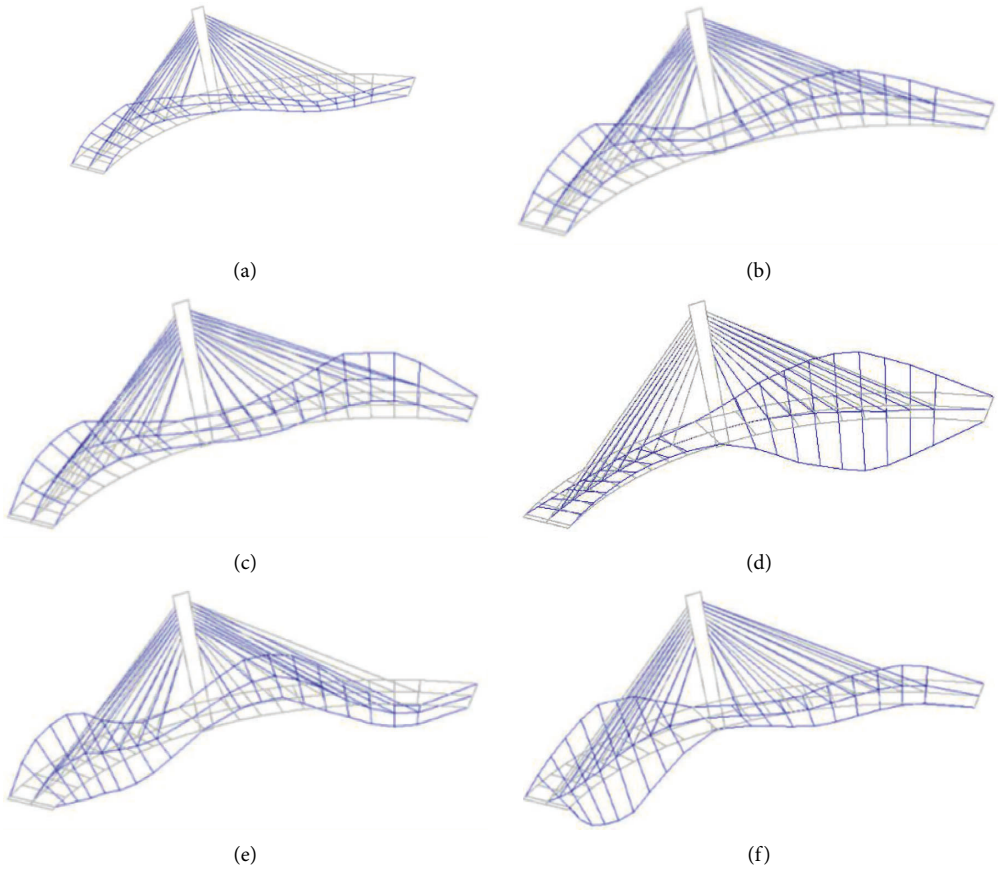

Figure 12: The representative experimental modes identified by the testing. (a) Mode 1 with $f = 0.635$ Hz. (b) Mode 2 with $f = 0.996$ Hz. (c) Mode 3 with $f = 1.143$ Hz. (d) Mode 4 with $f = 1.387$ Hz. (e) Mode 5 with $f = 1.523$ Hz. (f) Mode 6 with $f = 1.602$ Hz.

Table 6: Target values, reference/initial values, and updated values by the different methods.

Parameters		Direct method, round 1			Direct method, round 2		
	Target (GPa)	Ref. (GPa)	Results (GPa)	Relative error (%)	Ref. (GPa)	Results (GPa)	Relative error (%)
E_c	33	31	32.22	−2.38	34.65	36.3	10
E_s	205	210	225.5	10	215.3	196.8	−4
Parameters		Iterative method, round 1			Iterative method, round 2		
	Target (GPa)	Ini. (GPa)	Results (GPa)	Relative error (%)	Ini. (GPa)	Results (GPa)	Relative error (%)
E_c	33	31	32.19	−2.44	34.65	32.67	−1.00
E_s	205	210	196.20	−4.29	215.3	202.7	−1.12

identified in one of the two campaigns. Nevertheless, the MAC values are generally higher than 0.9 for almost all the identified mode shapes between the two campaigns. It suggested very high quality of the experimental results and less variation of the experimental conditions in 2010 and 2011. Finally, the first six modes identified by the testing are shown in Figure 12.

3.4. Comparison of the Two Methods Using Simulated Data. Both the direct updating method and the iterative updating method were first compared to each other on the key case study by using the simulated modal data as the target. The advantage of the simulated case study is that the exact solutions of the updating parameters are known. Two different rounds of the updating process were conducted by both methods, respectively, based on the different reference or initial values. The elastic modulus of the concrete slabs E_c and that of the steel girders E_S are chosen as the updating parameters. Their target values (exact solutions) are provided in Table 6. For both methods, the lower limits of E_S and E_C were assumed to be $0.9E_S^0$ and $0.9E_c^0$, respectively, and the upper limits of E_S and E_C were assumed to be $1.1E_S^0$ and $1.1E_c^0$, respectively. Herein, the superscript 0 denotes the reference/initial value. The choice of the reference/initial values and the corresponding updating results of both methods are summarized in Table 6. The relative error is defined as the difference between the result and the target values divided by the target one. It is observed that the results of the iterative method are less vulnerable to the changes of

Table 7: Comparison of the experimental and numerical data for the updated FE models with two parameters.

No.	*Mode*	f_{2010} (Hz)	$f_{FE\text{-}ini}$ (Hz)	$\Delta f_{FE\text{-}ini}$ (%)	MAC	$f_{FE\text{-}D}$ (Hz)	$\Delta f_{FE\text{-}D}$ (%)	MAC_D	$f_{FE\text{-}I}$ (Hz)	$\Delta f_{FE\text{-}I}$ (%)	MAC_I
1	B1	0.64	0.62	−2.5	0.96	0.62	−2.9	0.96	0.642	1.1	0.96
2	B2	1.00	0.91	−9.2	0.96	0.89	−10.8	0.96	0.96	−3.6	0.96
3	B3	1.14	1.10	−4.2	0.98	1.09	−4.5	0.98	1.133	−0.9	0.98
4	T1	1.39	1.38	−0.8	0.89	1.38	−0.9	0.91	1.433	3.3	0.92
5	M1	1.52	1.44	−5.4	0.96	1.44	−5.3	0.96	1.517	−0.4	0.96
6	T2	1.60	1.50	−6.5	0.88	1.50	−6.5	0.88	1.6	−0.1	0.88
7	B4	1.95	1.95	0.0	0.97	1.95	0.0	0.97	2.076	6.3	0.97
8	T3	2.64	2.53	−4.3	0.84	2.53	−4.2	0.87	2.704	2.5	0.82
9	T4	3.17	2.83	−10.7	0.93	2.83	−10.7	0.93	3.171	−0.1	0.94
10	T5	4.05	3.95	−2.6	0.95	3.94	−2.8	0.94	4.182	3.2	0.95
11	T6	4.93	4.77	−3.2	0.91	4.78	−3.2	0.91	5.034	2.1	0.91
12	T7	5.60	5.46	−2.4	0.95	5.47	−2.3	0.95	5.759	2.9	0.95
13	T8	6.83	6.67	−2.3	0.89	6.66	−2.4	0.90	7.006	2.6	0.92

Table 8: The selected parameters and their lower and upper limits.

No.	Parameters	Mean (GPa)	Min (GPa)	Max (GPa)
1	EEM of the pier	33	29.7	36.3
2	EEM of the pier cap	33	29.7	36.3
3	EEM of the base	33	29.7	36.3
4	EEM of the slab	33	29.7	36.3
5	EEM of the surface	33	29.7	36.3
6	EEM of pylon 1	28.2	25.4	31.0
7	EEM of pylon 2	28.2	25.4	31.0
8	EEM of pylon 3	28.2	25.4	31.0
9	EEM of pylon 4	28.2	25.4	31.0
10	EEM of the steel deck	210	189.0	231.0
11	EEM of the steel bracing	210	189.0	231.0

the initial values than those of the direct method. Moreover, more accurate results of the identified parameters can be achieved by using the iterative method. Similar conclusions were also provided by Smith et al. [28].

3.5. Finite Element Updating with Two Parameters. On the basis of the findings in the previous subsection, the experimental modal data were introduced as the target of FE updating for comparison of the two methods. Still only two updating parameters E_c and E_S are considered. The reference/initial values of E_S^0 and E_C^0 were, respectively, 205 GPa and 33 GPa for both the direct method and the iterative method. The solutions based on the direct method were found to be $E_S = 206$ GPa and $E_C = 31.35$ GPa. The solution based on the iterative method was found to be $E_S = 202.7$ GPa and $E_C = 32.67$ GPa. A summary of the numerical modal results of the updated FE models in comparison to the experimental counterparts is listed in Table 7. The subscripts *ini*, *D*, and *I* denote the initial model, the updated model with the direct method, and the updated model with the iterative method, respectively. f_{2010} represents the experimental natural frequencies obtained from testing in 2010. The MAC values were calculated between the experimental and the numerical mode shapes.

It is noted that, compared to the initial model, the updated model obtained from the iterative method is slightly improved with respect to the natural frequencies; meanwhile, the updated model obtained from the direct method is similar to the initial model with respect to the natural frequencies. In a greater detail, it is found that, for the initial model, $\Delta\overline{f}_{ini} = 5.13\%$. The value is improved to $\Delta\overline{f}_I = 2.80\%$ for the iterative method and however remains similar as $\Delta\overline{f}_D = 5.39\%$ for the direct method. The $\overline{MAC}$ values are almost unchanged as 0.93 for all the three models. So far it can be concluded that the iterative method can result in more accurate solutions of the updating parameters compared to the direct method. Concerning the modal data, normally the iterative method can lead to the models with higher accuracy compared to the direct method. Nevertheless, it should again be noted that the computational costs of the direct method remain relatively lower.

3.6. Finite Element Updating with Multiple Parameters. As the first step in calibration of the refined FE model with high fidelity, parametric analyses were performed to identify the most sensitive parameters affecting the FE model-computed modal frequencies and mode shapes. The changes in the selected parameters should potentially have a considerable effect on the global vibration response of the bridge rather than on local vibrations. Therefore, the material properties of the major structural components and the dimensions of those structural components are just some of

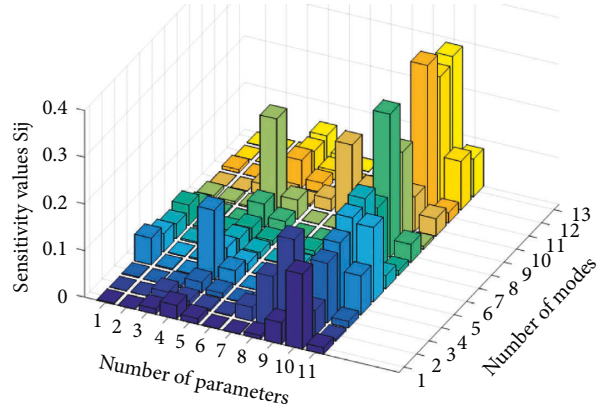

Figure 13: The sensitivity analysis of the selected parameters.

Table 9: Comparison of the experimental and numerical data for the updated FE models with four parameters.

No.	*Mode*	f_{2010} (Hz)	$f_{FE\text{-}ini}$ (Hz)	$\Delta f_{FE\text{-}ini}$ (%)	MAC	$f_{FE\text{-}D}$ (Hz)	$\Delta f_{FE\text{-}D}$ (%)	MAC_D	$f_{FE\text{-}I}$ (Hz)	$\Delta f_{FE\text{-}I}$ (%)	MAC_I
1	B1	0.64	0.62	−2.5	0.96	0.62	−1.8	0.96	0.64	0.8	0.96
2	B2	1.00	0.91	−9.2	0.96	0.93	−6.4	0.95	0.97	−3.0	0.95
3	B3	1.14	1.10	−4.2	0.98	1.1	−3.6	0.98	1.13	−1.2	0.98
4	T1	1.39	1.38	−0.8	0.89	1.33	−3.9	0.98	1.39	0.1	0.98
5	M1	1.52	1.44	−5.4	0.96	1.44	−5.4	0.97	1.49	−2.2	0.97
6	T2	1.60	1.50	−6.5	0.88	1.5	−6.6	0.9	1.54	−3.8	0.85
7	B4	1.95	1.95	0.0	0.97	1.95	−0.2	0.97	2	2.6	0.87
8	T3	2.64	2.53	−4.3	0.84	2.53	−4.2	0.97	2.63	−0.4	0.94
9	T4	3.17	2.83	−10.7	0.93	2.86	−9.9	0.93	2.98	−6.2	0.93
10	T5	4.05	3.95	−2.6	0.95	3.94	−2.8	0.94	4.1	1.2	0.94
11	T6	4.93	4.77	−3.2	0.91	4.77	−3.3	0.93	4.97	0.7	0.92
12	T7	5.60	5.46	−2.4	0.95	5.46	−2.4	0.95	5.69	1.7	0.95
13	T8	6.83	6.67	−2.3	0.89	6.62	−3.0	0.92	6.9	1.1	0.92

the potential parameters that can be selected for the FE model calibration. Besides, the parameters are selected among those whose exact values have high degrees of uncertainty [30]. In addition, any parameter of which the required information about its accurate values cannot be found should be considered. After a careful consideration of the initial FE model and the available engineering drawings, eleven parameters were selected in the bridge FE model to perform sensitivity analyses. These parameters were related to either boundary conditions or the mass and stiffness properties of the FE model. The selected parameters along with the lower and the upper limitations are listed in Table 8. In particular, the tower (pylon) was divided into four substructures, denoted by numbers 1–4 from the top to the bottom. The parametric mass of the bridge is easy to determine as compared to the parameters associated with the stiffness properties of the bridge. As a result, they were not considered as uncertain in the model updating.

Modal analyses were performed using the lower and upper limitations of the selected parameters listed in Table 8. The frequency values were obtained from the modal analysis of the FE model. The calculated sensitivity values for the 11 selected parameters are shown in Figure 13. It is found that the selected parameters nos. 4, 7, 9, and 10 in Table 8 are the most sensitive ones for the modal frequencies. After the most sensitive FE model parameters were identified, a brief study was done to investigate how variations in any of the 11 identified parameters change the numerical mode shapes. The upper limit values, lower limit values, and average values for each of the four parameters were used to obtain the FE-computed mode shapes. The mode shapes for the upper and lower bounds were compared to those extracted from the model using the mean values of the parameters. For comparison purposes, the MAC value is assessed between the mode shapes generated by varying one model parameter to one of its bounds (i.e., upper or lower) to the mode shapes associated with the model parameters set to their average values. The more the MAC value of a parameter study deviates from unity, the more sensitive the mode shape is to that parameter. It is found that the sensitivity results are in general similar in terms of the MAC values as compared to those measured in terms of the frequencies. It is then decided to use the four aforementioned parameters for updating the FE model.

The experimental modal data were introduced as the target of the FE updating for comparison of the two methods. The reference/initial values of the updating parameters are the mean values as given in Table 8. The weighting factors w_λ and w_z are equal to 1.0 and 2.0, respectively. The final finite element updated modal frequencies are presented in Table 9. The differences between the identified and initially calculated modal frequencies vary

in magnitude from 0% for the seventh mode to 10.7% for the ninth mode. It should be noted that the calculated translational modes have been neglected in the results as they were not investigated by the testing. A summary of the numerical modal results of the updated FE models in comparison to the experimental results is provided in Table 9. The subscripts *ini*, *D*, and *I* denote the initial model, the updated model with the direct method, and the updated model with the iterative method, respectively. f_{2010} represents the experimental natural frequencies. The *MAC* values were calculated between the experimental and the numerical mode shapes. It is noted that the updated model obtained with the iterative method is slightly improved ($\Delta\overline{f}_I = 2.50\%$) with respect to the natural frequencies as compared to the initial model ($\Delta\overline{f}_{ini} = 5.13\%$). Meanwhile the model that is obtained with the direct method is similar to the initial model with respect to the natural frequencies ($\Delta\overline{f}_D = 4.76\%$). Since the initial model already matches the experimental model results with relatively high *MAC* values ($\overline{MAC} = 0.93$), no significant improvement is observed for the updated models with either the direct method or the iterative method with respect to the model shapes. Overall, by using the iterative method, the updated models are generally more accurate compared to those of the direct method. Nevertheless, as compared to the experimental data, both methods can lead to the models with rather satisfactory modal results.

4. Conclusions and Future Perspectives

In this study, an operational modal testing and FE model updating of a conventional bridge with steel-concrete composite girder were conducted. Then, taking the curved Marghera bridge as the key case study, dynamic tests were performed. A highly refined finite element model was developed and calibrated based on the experimental results. Finally, the dynamic behavior of this curved steel-concrete composite cable-stayed bridge was studied based on the FE model with respect to the numerical methods for model updating. The main findings can be concluded as follows:

(1) Ambient vibration testing (or operational modal analysis) is a powerful technique for extracting experimental modal data of the bridges with either a conventional or a novel design concept. When proper measurement campaigns were organized, the vibration characteristics of the bridge could be identified with high accuracy and good reliability.

(2) During the FE model updating process, both the direct method (without iterations with respect to the numerical modal analysis) and the iterative method show a reliable performance for calibration of the refined baseline model which could serve on the purpose of the long-term monitoring of the structure.

(3) The direct method is usually more computationally efficient as compared to the iterative method. Both case studies of the straight composite bridge and the curved one give similar findings concerning the numerical efficiency. However, the more costly iterative method is a better choice when a good estimation of the reference point (the vector of the updating parameters) is not available. Moreover, the iterative method usually leads to the FE model with higher accuracy in comparison to the experimental data.

Future developments are expected regarding the further investigation of the dynamic behavior of the curved composite cable-stayed bridges by using the highly accurate FE model developed by this study. It concerns the effects of the different design choices, such as the curvature of the bridge, and those of the construction procedure, including the tuned cable forces.

Data Availability

The data used to support the findings of this study are available from the first author upon request.

Disclosure

This manuscript was modified based on the work presented in the thesis at https://iris.unica.it/handle/11584/266771, and the author of the thesis is the first author of this manuscript.

Conflicts of Interest

The authors declare that there are no conflicts of interest regarding the publication of this paper.

Authors' Contributions

Guanzhe Fa contributed to writing the original draft, visualization, and conceptualization. Leqia He contributed to numerical investigation, experimentation, and revision of the manuscript. Luigi Fenu contributed to supervision and guidance of the first author during his Ph.D. Bruno Briseghella contributed to supervision with review and editing.

Acknowledgments

The authors gratefully acknowledge the financial support from the National Natural Science Foundation of China (Grant no. 51778148). The authors would also like to thank Professor Carmelo Gentile, Polytechnic of Milan, for the valuable help and guidance in conducting the field tests of the Marghera bridge. Also they would like to thank the technicians (M. Antico and M. Cucchi) of the VIBLAB Laboratory of Vibrations and Dynamic Monitoring of Structures, Polytechnic of Milan, for the valuable help in conducting the field tests. The corresponding author wants to thank Professor Guido De Roeck for the guidance during his post-doctoral research period at KUL and Prof. Edwin Reynders for the valuable discussions on the research topic.

References

[1] M. Virlogeux, "Recent evolution of cable-stayed bridges," *Engineering Structures*, vol. 21, no. 8, pp. 737–755, 1999.

[2] S. Sehgal and H. Kumar, "Structural dynamic model updating techniques: a state of the art review," *Archives of Computational Methods in Engineering*, vol. 23, no. 3, pp. 515–533, 2016.

[3] B. Briseghella, G. Fa, A. Aloisio et al., "Dynamic characteristics of a curved steel–concrete composite cable-stayed bridge and effects of different design choices," *Structures*, vol. 34, pp. 4669–4681, 2021.

[4] S. Heyrani Moghaddam and A. Shooshtari, "An energy balance method for seismic analysis of cable-stayed bridges," *Proceedings of the Institution of Civil Engineers-Structures and Buildings*, vol. 172, no. 12, pp. 871–881, 2019.

[5] D. H. Choi, H. Yoo, J. I. Shin, S. I. Park, and K. Nogami, "Ultimate behavior and ultimate load capacity of steel cable-stayed bridges," *Structural Engineering & Mechanics*, vol. 27, no. 4, pp. 477–499, 2007.

[6] M. M. Hassan, "Optimization of stay cables in cable-stayed bridges using finite element, genetic algorithm, and B-spline combined technique," *Engineering Structures*, vol. 49, pp. 643–654, 2013.

[7] K. Wei, H. He, J. Zhang, C. Yang, and S. Qin, "An endurance time method-based fragility analysis framework for cable-stayed bridge systems under scour and earthquake," *Ocean Engineering*, vol. 232, Article ID 109128, 2021.

[8] S. Kim and Y. J. Kang, "Structural behavior of cable-stayed bridges after cable failure," *Structural Engineering & Mechanics*, vol. 59, no. 6, pp. 1095–1120, 2016.

[9] S. Kim, D. H. Won, and Y. J. Kang, "Ultimate behavior of steel cable-stayed bridges-I. Rational ultimate analysis method," *Int J Steel Struct*, vol. 16, no. 2, pp. 601–624, 2016.

[10] S. Kim, D. H. Won, and Y. J. Kang, "Ultimate behavior of steel cable-stayed bridges-II. Parametric study," *International Journal of Steel Structures*, vol. 16, no. 2, pp. 625–636, 2016.

[11] M. Bhagwat, S. Sasmal, B. Novak, and A. Upadhyay, "Dynamic performance evaluation of straight and curved cable-stayed bridges," *Bridge Structures*, vol. 5, no. 2-3, pp. 87–95, 2009.

[12] F. Ferreira and L. Simões, "Least cost design of curved cable-stayed footbridges with control devices," *Structures*, vol. 19, pp. 68–83, 2019.

[13] T. Zordan, B. Briseghella, and T. Liu, "Finite element model updating of a tied-arch bridge using Douglas-Reid method and Rosenbrock optimization algorithm," *Journal of Traffic and Transportation Engineering*, vol. 1, no. 4, pp. 280–292, 2014.

[14] E. Reynders, G. D. Roeck, P. Gundes Bakir, and C. Sauvage, "Damage identification on the Tilff Bridge by vibration monitoring using optical fiber strain sensors," *Journal of Engineering Mechanics*, vol. 133, no. 2, pp. 185–193, 2007.

[15] M. Friswell and J. E. Mottershead, *Finite Element Model Updating in Structural Dynamics*, Vol. 38, Springer Science & Business Media, , Berlin, Germany, 1995.

[16] R. J. Allemang, "The modal assurance criterion–twenty years of use and abuse," *Sound and Vibration*, vol. 37, no. 8, pp. 14–23, 2003.

[17] A. Araujo, J. García-Palacios, J. Blesa et al., "Wireless measurement system for structural health monitoring with high time-synchronization accuracy," *IEEE Transactions on Instrumentation and Measurement*, vol. 61, no. 3, pp. 801–810, 2012.

[18] E. Reynders, M. Schevenels, and G. D. ROECK, *MACEC 3.2: A MatLab Toolbox for Experimental and Operational Modal Analysis. Report BWM-2011-01*, Katholieke Universiteit Leuven, Belgium Europe, 2011.

[19] B. Peeters and G. De Roeck, "Reference-based stochastic subspace identification for output-only modal analysis," *Mechanical Systems and Signal Processing*, vol. 13, no. 6, pp. 855–878, 1999, mssp.1999.1249.

[20] E. Reynders, R. Pintelon, and G. De Roeck, "Uncertainty bounds on modal parameters obtained from stochastic subspace identification," *Mechanical Systems and Signal Processing*, vol. 22, no. 4, pp. 948–969, 2008 May 1.

[21] G. Fa, *Dynamic behaviour of curved cable-stayed bridges*, PhD Thesis, University of Cagliari, Cagliari Italy, 2016.

[22] J. E. Mottershead, M. Link, and M. I. Friswell, "The sensitivity method in finite element model updating: a tutorial," *Mechanical Systems and Signal Processing*, vol. 25, no. 7, pp. 2275–2296, 2011.

[23] A. A. Mosavi, H. Sedarat, S. M. O'Connor, A. Emami-Naeini, and J. Lynch, "Calibrating a high-fidelity finite element model of a highway bridge using a multi-variable sensitivity-based optimisation approach," *Structure and Infrastructure Engineering*, vol. 10, no. 5, pp. 627–642, 2014.

[24] B. Briseghella, T. Zordan, C. Lan, E. Mazzarolo, F. Busatta, and C. Gentile, "Safety Monitoring of the Cable Stayed Bridge in the Commercial Harbor of Venice," in *Proceedings of the Fifth International Conference on Bridge Maintenance IABMAS 2010 Conference*, Philadelphia, USA, July 2010.

[25] C. Gentile and E. Siviero, "Dynamic characteristics of the new curved cable-stayed bridge in Porto Marghera (Venice, Italy) from ambient vibration measurements," *InIMAC-XXV*, pp. 1–10, 2007.

[26] B. Briseghella, A. Del Grosso, C. Gentile, E. Siviero, A. Torre, and T. Zordan, "Reception test and monitoring system of the new Marghera cable-stayed bridge in the harbour of Venice," in *Proceedings of the Internationa Symposium on Integrated Life-Cycle Design and Management of Infrastructure*, pp. 1–12, Shanghai China, May 2007.

[27] B. Briseghella, G. Fa, A. Aloisio et al., "Dynamic characteristics of a curved steel–concrete composite cable-stayed bridge and effects of different design choices," in *Structures*vol. 34, pp. 4669–4681, Elsevier, 2021.

[28] S. W. Smith and C. A. Beattie, "Secant-method adjustment for structural models," *AIAA Journal*, vol. 29, no. 1, pp. 119–126, 1991.

[29] E. Simoen, G. De Roeck, and G. Lombaert, "Dealing with uncertainty in model updating for damage assessment: a review," *Mechanical Systems and Signal Processing*, vol. 56-57, pp. 123–149, 2015.